Catalysis Science & Technology

Accepted Manuscript

Catalysis
Science &
Technology

rsc.li/catalysis

Volume 7
Number 2
21 January 2017
Pages 313-534

ISSN 2044-4761

ROYAL SOCIETY
OF CHEMISTRY

PAPER
Chaoqiu Chen, Yong Qin et al.
Highly dispersed Pt nanoparticles supported on carbon nanotubes produced by atomic layer deposition for hydrogen generation from hydrolysis of ammonia borane

This is an Accepted Manuscript, which has been through the Royal Society of Chemistry peer review process and has been accepted for publication.

Accepted Manuscripts are published online shortly after acceptance, before technical editing, formatting and proof reading. Using this free service, authors can make their results available to the community, in citable form, before we publish the edited article. We will replace this Accepted Manuscript with the edited and formatted Advance Article as soon as it is available.

You can find more information about Accepted Manuscripts in the Information for Authors.

Please note that technical editing may introduce minor changes to the text and/or graphics, which may alter content. The journal's standard Terms & Conditions and the Ethical guidelines still apply. In no event shall the Royal Society of Chemistry be held responsible for any errors or omissions in this Accepted Manuscript or any consequences arising from the use of any information it contains.

ROYAL SOCIETY
OF CHEMISTRY

rsc.li/catalysis

Paper

Catalysis to discriminate single atoms from subnanometric ruthenium particles in ultra-high loading catalysts

C. Rivera-Cárcamo,[a] F. Leng,[a] I. C. Gerber,[b] I. del Rosal,[b] R. Poteau,[b] V. Collière,[a] P. Lecante,[c] D. Nechiyil,[c] W. Bacsa,[c] A. Corrias,[d] M. R. Axet,[a] and P. Serp[*a]

We report a procedure for preparing ulta-high metal loading (10-20 % w/w Ru) Ru@C_{60} nanostructured catalysts comprising exclusively Ru single atoms. We show that by changing the Ru/C_{60} ratio and the nature of the solvent used during the synthesis, it is possible to increase the Ru loading up to 50% w/w, and to produce hetero-structures containing subnanometric Ru nanoparticles. Several techniques such as high-resolution transmission electron microscopy (HRTEM), scanning transmission electron microscopy – high angle annular dark field (STEM-HAADF), Raman spectroscopy, wide-angle X-ray scattering (WAXS), extended X-ray absorption fine structure (EXAFS) and X-ray photoelectron spectroscopy (XPS) together with theoretical calculations were used to characterize these materials. At such high metal loading, the distinction between Ru single atoms and clusters is not trivial, even with this combination of techniques. We evaluated the catalytic properties of these materials for the hydrogenation of nitrobenzene and 2,3-dimethyl-2-butene. The catalysts containing only Ru single atoms are much less active for these reactions than the ones containing clusters. For nitrobenzene hydrogenation, this is because electro-deficient Ru single atoms and few atom Ru_n clusters are not performant for H_2 activation compared to larger clusters (n ≥ 13), as shown by density functional theory (DFT) calculations. For the more crowded substrate 2,3-dimethyl-2-butene, DFT calculations have shown that this is due to steric hindrance. These simple tests can thus been used to distinguish samples containing metallic sub-nanometer nanoparticles. These novel catalysts are also extremely active for the hydrogenation of -substituted 2,3-dimethyl-2-butene.

Introduction

Extensive research is currently devoted to the reproducible synthesis of supported subnanometric metal particles[1] and even single atoms (SA).[2-4] This is due to the specific physicochemical properties of these species compared to bulk metal but also to nanometric particles,[1, 5] which open the route through applications in many fields such as quantum technologies, sensors, energy, environment, biology or catalysis.[6-8] In the last few years, various strategies for dispersing metal SA on supports have emerged.[9] Except for metal organic frameworks, which can be used as precursors for preparing SA catalysts,[10-12] in most of the cases low metal loadings have been reached, and it is currently very challenging to guarantee a loading content high enough for practical applications. Taking advantage of solution chemistry

it is today possible to prepare atomically precise metal clusters, but mainly with few metals such as gold or silver.[13-19] The formation of these clusters necessarily requires stabilization to prevent aggregation, which would eradicate most of their desirable properties compared with bulk materials of identical composition. Additionally, for many applications these objects have to be integrated into a system, so the preparation of assemblies of subnanometric metal particles linked by strong covalent bonds could solve this problem. Very few strategies have been proposed to prepare such assemblies. One example is Pd-polymer micelles containing 0.7 nm Pd clusters, which have been prepared by ligand exchange from [Pd(PPh$_3$)$_4$].[20] From these observations, it appears that the development of simple synthetic strategies to produce nanoarchitectures with SA and/or subnanometric particles, with significant metal loading, is particularly appealing and challenging.

Fullerene C_{60} is an interesting building block to stabilize single metal atoms or nanoparticles (NP). Indeed, the high degree of symmetry, the strong tendency toward polymerization of this molecule, and its coordinating geometries make it an ideal candidate for the construction of well-defined nanostructures.[21] In transition metal fullerides, depending on the amount of metal, the suggested structure could be polymeric with a chain-like -(M$_1$@C_{60})$_n$- arrangement of metal single atoms, or with two- or three-dimensional

[a.] LCC-CNRS, Université de Toulouse, UPR 8241 CNRS, INPT, Toulouse, France
[b.] Université de Toulouse; INSA, UPS, CNRS; LPCNO (IRSAMC), 135 avenue de Rangueil, F-31077 Toulouse, France
[c.] Centre d'élaboration des matériaux et d'études structurales UPR CNRS 8011, 29 Rue Jeanne-Marvig, BP 4347, 31055 Toulouse, France
[d.] School of Physical Sciences, Ingram Building, Room 118, University of Kent Canterbury, CT2 7NH, UK
† Footnotes relating to the title and/or authors should appear here.
Electronic Supplementary Information (ESI) available: [details of any supplementary information available should be included here]. See DOI: 10.1039/x0xx00000x

Paper

coordination.[22, 23] Palladium,[24-26] and more recently ruthenium[27] spherical nanostructures containing SA have been produced. For Pd, it has been proposed that the synthesis of Pd fullerides can produce structures containing isolated Pd atoms with a stoichiometry between Pd_1C_{60} and $Pd_{4.9}C_{60}$.[24, 28] However, a closer inspection of the literature data for the Pd-C_{60} system shows that these syntheses are sensitive to the experimental conditions and not selective. In the cases in which HRTEM was used to characterize the reaction products, metallic Pd NP were also observed, even at low Pd/C_{60} ratio.[26, 29] If a Pd_3C_{60} fulleride has indeed been produced and characterized,[25, 26] when a Pd/C_{60} ratio of 3 was used, it was not the only product of the reaction, and also significant amount of NP (5-20 nm) were observed. DFT calculations have suggested that both isolated atoms and weakly bonded metal aggregates may exist in equilibrium.[30] EXAFS analyses have allowed to propose the presence of Pd clusters in Pd_3C_{60},[31] and XRD analyses have shown the presence of metallic Pd, starting from composition Pd_2C_{60} and higher.[25] From these results, it seems that if the kinetic product of the reaction, the -(Pd_1C_{60})- polymer, is rapidly formed, the incorporation of additional Pd in the structure is not straightforward. We suspect that diffusional limitations should prevail, which may lead to Pd clusters or NP formation on the surface of the -(Pd_1C_{60})- polymer. We obtained similar results in the case of ruthenium.[27] It therefore appears difficult to produce fulleride metal-clusters, and this must be linked to the fact that once the kinetic product of the reaction is formed (the nanostructures containing SA), the additional ruthenium is deposited on the external surface of the spheres because it cannot diffuse in the porosity of the spheres. Thus, if C_{60} fullerene-metal cluster complexes are well known for many years,[32] up to now, C_{60} metal-cluster fullerides are essentially hypothetical.[33]

In this work we tried to overcome this difficulty by using mixtures of solvents during the synthesis so as to favor the deposit of ruthenium in the porosity of the -(Ru_1@C_{60})-n materials so as to obtain -(Ru_n@C_{60})n- metal-cluster fullerides. Thus, we report the straightforward self-assembly synthesis of Ru SA and Ru subnanometric particles with C_{60}. These structures, characterized by a very high Ru loading (up to 50 % w/w Ru) have been characterized by a large variety of techniques, including STEM-HAADF, WAXS, EXAFS, XPS and Raman spectrometry, and tested as catalysts for hydrogenation reactions. We have demonstrated that the presence of clusters can be easily detected by performing hydrogenation test on nitrobenzene (NB) or 2,3-dimethyl-2-butene. While Ru single atoms are poorly active for electronic but also steric reasons, as soon as metallic assemblies are present, the activity increases. We have also shown that the subnanometric Ru particles are highly active hydrogenation catalysts and are able to efficiently catalyze hydrogenation of the tetrasubstituted olefin 2,3-dimethyl-2-butene.

Experimental

General methods

All operations were carried out under argon atmosphere using standard Schlenk techniques or in an MBraun glovebox. Solvents were purified by standard methods or by an MBraun SPS-800 solvent purification system. [Ru(COD)(COT)] (COD= 1,5 cyclooctadiene, COT= 1,3,5-cyclooctatriene) was purchased from Nanomeps Toulouse, fullerene C_{60} from Sigma-Aldrich, Ar and H_2 from Air Liquid. All these reactants were used as received. The ruthenium content was established by inductively coupled plasma optical emission spectroscopy (ICP-OES) with a Thermo Scientific ICAP 6300 instrument on samples dried 2 h at 200 °C.

Synthesis of Ru@C_{60} nanostructures

In a typical experiment the [Ru(COD)(COT)] complex was introduced in a Fisher-Porter bottle with a solution of fullerene C_{60} in the desired solvent. The resulting purple solution was stirred for 30 min at room temperature, after which the bottle was pressurized with 3 bar of H_2. The solution, which turned black after few minutes of reaction, was kept under stirring overnight at room temperature. After this period, excess of H_2 was eliminated and the volume of solvent was reduced under vacuum. Pentane was then added to precipitate the colloidal suspension. After filtration under argon with a cannula, the black solid was washed twice with pentane and filtrated again before drying under vacuum. The quantities of reactant used for each Ru/C_{60} ratio studied are detailed in S0.

Hydrogenation of nitrobenzene

Hydrogenation reactions were performed in Top Industry high pressure and temperature Stainless steel autoclave with a controlling system. In a typical experiment, the autoclave was purged by three vacuum/argon cycles. The mixture of Ru@C_{60} catalysts (0.025 mmol Ru), dodecane (as internal standard, 1.1 mmol) and nitrobenzene (4.06 mmol) in 30 mL of ethanol was prepared in a glovebox, ultrasonicated for 5 min and then transferred into a high-pressure autoclave under argon atmosphere. The autoclave was heated to 80 °C and pressurized with 30 bar of H_2; the stirring rate was fixed at 1000 rpm. Samples of the reaction mixture were taken periodically and then analysed by GC-MS. Quantitative analysis of reaction mixtures was performed via GC-MS using calibration solutions of commercially available products.

Hydrogenation of 2,3-dimethyl-2-butene

In a typical experiment, the Top Industry autoclave was purged by three vacuum/argon cycles. The mixture of Ru@C_{60} catalysts (5 mg), dodecane (as internal standard, 1.1 mmol) and 2.3-dimethyl-2-butene (10.0 mmol) in 30 mL of cyclohexane was prepared in a glovebox, ultra-sonicated for 5 min and then transferred into a high-pressure autoclave under argon atmosphere. The autoclave was heated to 50 °C and pressurized with 20 bar of H_2; the stirring rate was fixed at 1000 rpm. Samples of the reaction mixture were taken periodically and then analysed by GC-MS. Quantitative analysis of reaction mixtures was performed via GC-MS using calibration solutions of commercially available products.

Nanoscale   **Paper**

Catalyst characterization

TEM analyses. TEM and HRTEM analyses were performed at the "Centre de microcaracterisation Raimond Castaing, UMS 3623, Toulouse". Low resolution TEM was performed by using a JEOL JEM 1011 CX-T electron microscope operating at 100 kV with a point resolution of 4.5 Å, and a JEOL JEM 1400 electron microscope operating at 120 kv. The high resolution analyses were conduct using a JEOL JEM 2100F equipped with a Field Emission Gun (FEG) operating at 200 kV with a point resolution of 2.3 Å and a JEOL JEM-ARM200F Cold FEG operating at 200 kV with a point resolution of > 1.9 Å. The approximation of the particles mean size was made through a manual analysis of enlarged micrographs by measuring at least 200 particles on a given grid. Other TEM micrographs were acquired with a JEOL 2100F S/TEM microscope equipped with a FEG operating at 200 kV, a spherical aberration probe corrector and a GATAN Tridiem energy filter. The resolutions attained are 2 Å and 1.1 Å under parallel TEM mode and scanning STEM modes, respectively. For STEM-HAADF analyses the spot size was of 0.13 nm, a current density of 140 pA, the camera focal length was 10 cm, corresponding to inner and outer detection angle of the annular detector of about 60 mrad and 160 mrad.

WAXS, EXAFS, Raman and XPS analyses. Wide Angle X-ray Scattering measurements were performed at CEMES on a diffractometer dedicated to Pair Distribution Function (PDF) analysis: graphite-monochromatized Molybdenum radiation (0.07169 nm), solid-state detection and low background setup. Samples sealed in Lindemann glass capillaries (diameter 1.5mm) to avoid any oxidation after filling in a glove box. For all samples data were collected on an extended angular range (129 degrees in 2 theta) with counting times of typically 150s for each of the 457 data points, thus allowing for PDF analysis. Classic corrections (polarization and absorption in cylindrical geometry) were applied before reduction and Fourier transform. The X-ray absorption spectra were recorded on the B18 beamline at the DIAMOND synchrotron (Oxfordshire, UK). Extended X-ray Absorption Fine Structure (EXAFS) spectra at the Ru (22117 eV) K-edge were collected at room temperature in transmission mode using a Si(311) monochromator. The monochromator energy scale was calibrated *via* a third ion chamber with a reference foil. The samples, in form of powder, were diluted with polyvinylpyrrolidone (PVP) in an appropriate concentration inside a glove box and pressed to form a pellet, which was then sealed in an aluminum pouch to avoid any oxidation. The data analysis was performed using the ATHENA and ARTEMIS software.[34] With ATHENA, the absorption edge, E0, is determined, and the absorption due to the isolated atom is subtracted, by fitting the pre-edge and post-edge regions to obtain $\chi(k)$. The software ARTEMIS is used to perform the fit of the EXAFS region to scattering models in R-space obtained by FEFF, validated on standard compounds. The number of fitted parameters was always lower than the number of independent points. Raman measurements were carried out with a Horiba XPLORA-MV2000 spectrometer. For the measurements, an excitation wavelength of 532 nm and laser power of 0.084 mW was used. The samples were kept under vacuum and exposed to atmospheric air shortly before measurements. The samples were analyzed by X-ray photoelectron spectroscopy (XPS) using a VG Escalab MKII spectrophotometer operating with a non monochromatized Mg K source (1253.6 eV).

Density Functional Theory (DFT) calculations

Calculations were performed using the Vienna *ab initio* simulation package VASP,[35-39] which employs the full-potential projector augmented waves (PAW) framework.[39, 40] Exchange-correlation effects were approximated using the PBE functional and applied in spin-polarized calculations.[41] A kinetic energy cutoff of 400 eV was found to be sufficient to achieve a total energy convergence within several meV, in conjunction with a k-point sampling grid of (1x1x4), by applying a 0.05 eV-width Gaussian smearing, on the various Ru_n-C_{60} polymer phase models, based on the models already proposed in a previous work, that satisfy Ru/C_{60} ratio and may represent only an idealized view of the real system.[27] All atoms were fully relaxed in order to have forces smaller than 0.01 $eV/Å^{-1}$. The calculation cell parameters were at least equal to 21 Å on the (*Ox,Oy*) directions when on (*Oz*) it was dependent on the Ru cluster sizes. See Fig. S1 for more details. Bader charge analysis was used to estimate charge transfer.[42, 43] Transition state searches were performed using the Nudge Elastic Band method, as implemented by Henkelman et al.,[44, 45] on a molecular models made of a fully hydrogenated Ru_{13} NP decorated by two C_{60} ligands.

Results and discussion

$Ru@C_{60}$ hetero-structure synthesis and TEM characterization

$Ru@C_{60}$ hetero-structures were synthesized by decomposing [Ru(COD)(COT)] under H_2 (3 bar) in the presence of C_{60} at room temperature. The reaction conditions for each sample, the resulting metal loading, and the Ru NP size are summarized in Table 1. Several solvents and mixtures of solvents were used to synthesize the hetero-structures, and it had a pronounced influence on the shape of the structures produced (Fig. S2). We already reported that for a 1/1 Ru/C_{60} ratio, nanospheres (30-40 nm, Fig. S2a) are produced in pure CH_2Cl_2 (entry 1, Table 1, $D-Ru_1@C_{60}$), while the reaction conducted in pure toluene yields a nanostructure of undefined shape (entry 4, Table 1, $T-Ru_1@C_{60}$, Fig. S2c).[27] These $Ru_1@C_{60}$ structures constitute the kinetic product of the reaction and contain only Ru single atoms (Fig. S2b,d) connected by C_{60} with a η^2-η^6 coordination.[27] We have attributed this difference of morphology to the fact that C_{60} are much more soluble in toluene (2.80 mg/mL) than in CH_2Cl_2 (0.26 mg/mL). Indeed, it is known that self-assembly mainly based on specific amphiphilicity in a surrounding medium, may results in a selection of morphologies.[46] For a Ru/C_{60} ratio of 2/1 in CH_2Cl_2 (entry 2, Table 1), the polymeric spheres are already covered by a shell of 1.2 nm size Ru NP (Fig. S3a,b), whose thickness increases with the increase of the Ru/C_{60} ratio.[27] Theoretically based on thermodynamics arguments, the formation of Ru clusters and Ru NP is favored over the increase of number of single atoms.

Paper

Table 1. Loading and mean particle size of the Ru@C_{60} samples

Entry	Ru@C_{60} samples	Solvent	Temperature (°C)	Ru loading (%)[a]	Ru NP size (nm)
1	D-Ru$_1$@C_{60} 1/1[27]	CH_2Cl_2	25	10.6 (12.3)	n. d.[b]
2	D-Ru@C_{60} 2/1[27]	CH_2Cl_2	25	16.7 (21.9)	1.2 ± 0.1
3	D-Ru@C_{60} 5/1[27]	CH_2Cl_2	25	35.6 (41.2)	1.3 ± 0.1
4	T-Ru$_1$@C_{60} 1/1[27]	Toluene	25	9.1 (12.3)	n. d.
5	T-Ru@C_{60} 5/1	Toluene	25	11.0 (41.2)	n. d.
6	T-Ru@C_{60} 10/1	Toluene	25	16.6 (58.3)	n. d.
7	T-Ru@C_{60} 20/1	Toluene	25	20.0 (73.7)	n. d.
8	T-Ru@C_{60} 40/1	Toluene	25	19.2 (84.8)	n. d.
9	T-Ru@C_{60} 20/1	Toluene	50	19.6 (73.7)	n. d.
10	T-Ru@C_{60} 20/1	Toluene	100	20.5 (73.7)	n. d.
11	T$_{95}$D$_5$-Ru@C_{60} 20/1	Toluene (95%)/CH_2Cl_2 (5%)	25	24.4 (73.7)	n. d.
12	T$_{75}$D$_{25}$-Ru@C_{60} 20/1	Toluene (75%)/CH_2Cl_2 (25%)	25	35.8 (73.7)	n. d.
13	T$_{50}$D$_{50}$-Ru@C_{60} 20/1	Toluene (50%)/CH_2Cl_2 (50%)	25	36.0 (73.7)	suspected
14	T$_{95}$M$_5$-Ru@C_{60} 20/1	Toluene (95%)/MeOH (5%)	25	34.7 (73.7)	suspected
15	T$_{75}$M$_{25}$-Ru@C_{60} 20/1	Toluene (75%)/MeOH (25%)	25	41.6 (73.7)	suspected
16	T$_{50}$M$_{50}$-Ru@C_{60} 20/1	Toluene (50%)/MeOH (5 %)	25	47.1 (73.7)	suspected

[a] From ICP analyses. The value between parentheses is the theoretical Ru loading considering the initial amount of it. [b] n. d. = not detected

Indeed even if the coordination energy between one Ru atom and two C_{60} is 84 kcal/mol, the cohesive energy per Ru atom in naked Ru$_{13}$ is -96 kcal/mol or -90 kcal/mol in the -(Ru$_2$@C_{60})$_n$- model, as in Fig.S1 Despite the fact that we cannot completely exclude the formation complex 2D or 3D structures since they appear to be stable when increasing the metal/carbon ratio,[22] it seems that the electronic structures of various transition metals embedded in more structured systems remain very similar to the 1D case. As a consequence in our models we will retain only the wire configuration.[47]

This result is consistent with the fact that the -(D-Ru$_1$@C_{60})$_n$- polymer does not swell in CH_2Cl_2, so that the additional Ru atoms cannot be incorporated in the structure due to diffusional limitations, and nucleation occurs on the surface of the nanospheres. The polymer swelling could favor the incorporation of additional Ru in the structure, and cluster/NP formation. Indeed, experimental evidence has shown the importance of polymer swelling in the diffusion process,[48] the swelling process controlling the diffusion rate.

Interestingly, using pure toluene as solvent, no Ru NP are visible from HRTEM and STEM-HAADF images even for a 5/1 Ru/C_{60} ratio (entry 5, Table 1, and Fig. S3c-e). We noticed however that the final Ru loading is lower in toluene than in dichloromethane at the same Ru/C_{60} ratio (Table 1). In order to increase the Ru loading we firstly increased the Ru/C_{60} ratio (entries 4-8, Table 1). By increasing the Ru/C_{60} ratio from 1/1

to 40/1, only a moderate increase in Ru loading was obtained, and a plateau is reached at 20 % w/w Ru. We also investigated the effect of the temperature (entries 7, 9 and 10, Table 1). An increase of the temperature of reaction from 25 to 100 °C for a Ru/C_{60} ratio of 20/1 does not allow increasing the Ru loading above 20% w/w. It is however important to notice that, contrarily to the sample D-Ru@C_{60} 2/1 (16.7% Ru w/w),[27] at 20 % w/w Ru loading, the sample produced in toluene does not contain any Ru NP from HRTEM and STEM-HAADF observations (Fig. S4). This result is consistent with a swelling of the T-Ru$_1$@C_{60} sample that allows incorporation of additional Ru atoms. Retention of toluene due to swelling in -(T-Ru$_1$@C_{60})$_n$- polymeric particles was detected from TGA analyses (Fig. S.5). It has already been reported that the fullerene polymer-like materials, C_{60}Pd$_n$, showed good adsorptivity toward toluene.[49]

We discovered that the existence of the plateau is connected to the rapid formation of a stable complex (1,5-cyclooctadiene)(toluene)Ru(0) in solution by the reaction of the solvent with the ruthenium precursor. The formation of this species in the medium has been confirmed by NMR, and this complex was isolated from the yellow filtrates obtained at the end of the reactions (Fig. S6). We independently synthesized this complex,[50] and confirmed that it hardly reacts in the presence of C_{60} and dihydrogen at 25°C.

Paper

After 24 h reaction, a black solid is obtained in low yield (16 %) that contains only 6 % Ru w/w. In order to limit the formation of [Ru(COD)(toluene)] and to increase the Ru loading we investigated for the first time the use of solvent mixtures with toluene. Two solvents have been investigated, CH_2Cl_2 (entries 11-13, Table 1) and methanol (entries 14-16, Table 1), which can act as coordinating solvents to the Ru atoms to limit the formation of the stable Ru complex with toluene.[51, 52] The use of toluene/CH_2Cl_2 mixtures (50/50) allows increasing the Ru loading (for a Ru/C_{60} ratio = 20) from 20 to 36%. The Ru loading reaches 34.7% for a toluene/methanol mixture (95/5), and 47.1 % for a toluene/methanol mixture (50/50). The sample $T_{95}D_5$-Ru@C_{60} 20/1 was analyzed by STEM-HAADF (Fig. S7). The EDX profiles of this specific sample show a higher content of Ru on the nanostructure surface indicating that a core-shell structure starts to develop, with a Ru rich shell (Fig. S7d). However, at these high Ru loading, the detection of Ru NP was not straightforward. The sample $T_{95}M_5$-Ru@C_{60} 20/1 was also observed by STEM-HAADF and no Ru NP was clearly observed (Fig. S8), but no core-shell structure was formed. So we can propose that for the samples prepared in toluene/methanol mixture, the extra Ru atoms are incorporated into the hetero-structure to provide more Ru atoms or subnanometric Ru particles.

For the $T_{50}D_{50}$-Ru@C_{60} sample, presenting a similar metal loading than $T_{95}M_5$-Ru@C_{60} (Table 1, entries 13 and 14), the formation of core-shell spherical particles is clearly observed (Fig. 1a,b), on which the extra Ru atoms have the tendency to deposit on the external surface of the spheres (see Fig. 1a for EDX mapping). There also, the structuration of Ru as metallic NP was not clear (Fig. 1b). Finally, for the $T_{50}M_{50}$-Ru@C_{60} 20/1 sample, no core shell structure was produced (Fig. 1c-d), and once again the detection of metallic NP was not easy due to the extremely high Ru loading (47 % w/w, which corresponds to 6 Ru atoms for 1 C_{60}). From these results, it appears that the use of solvent mixtures during the synthesis impacts the fate of the reaction. First, the use of toluene/CH_2Cl_2, and particularly of toluene/CH_3OH mixtures allows to significantly increase the Ru loading, which reaches almost 50 % w/w in the $T_{50}M_{50}$-Ru@C_{60} sample. This could be attributed to a competition between the solvents for coordination to Ru, and to the generation of Ru intermediate species that are more easily decomposed than the stable [Ru(COD)(toluene)] complex. An easier coordination of methanol compared to dichloromethane is not surprising. Second, the choice of the second solvent (CH_2Cl_2 or CH_3OH) has also an impact on Ru location. The use of CH_2Cl_2 does not allow depositing the extra Ru inside the hetero-structure and a shell of Ru species are deposited around the -(Ru$_1$@C_{60})$_n$- core.
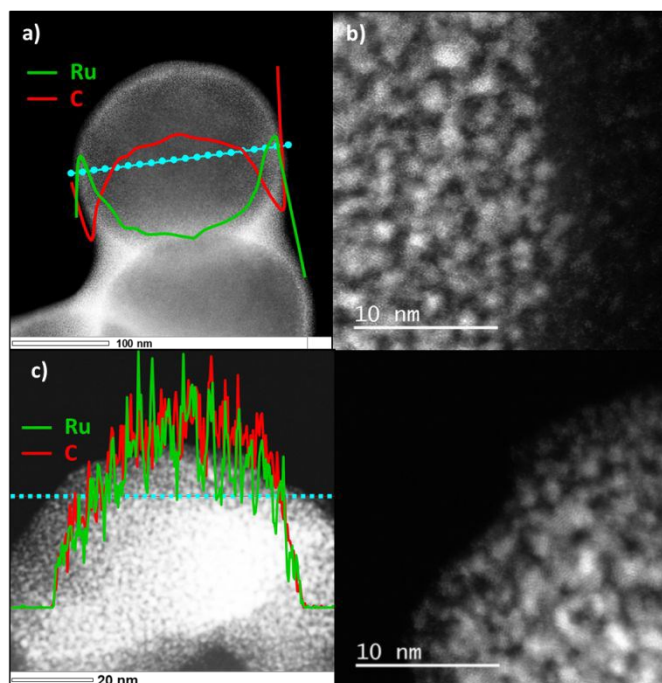

Fig. 1. a), b) STEM-HAADF micrographs and EDX mapping of the $T_{50}D_{50}$-Ru@C_{60} sample; and c), d), STEM-HAADF micrographs and EDX mapping of the $T_{50}M_{50}$-Ru@C_{60} sample.

When CH_3OH is used, the extra Ru atoms are incorporated inside the hetero-structure. We propose that it is the swelling of the -(Ru$_1$@C_{60})$_n$- product that allows the incorporation of extra Ru atoms inside the hetero-structure. Methanol should act as a porogen (pore generating solvent) for the -(Ru$_1$@C_{60})$_n$-structure. In polymer chemistry, the porogen is the most influencing parameter to the surface area, porosity, and morphology of the polymer.[53] Finally, it is worth mentioning that if the presence of Ru subnanometric particles could be suspected in samples prepared using mixtures of solvents (up to 6 Ru atoms for 1 C_{60}), the high metal loadings makes their identification by STEM-HAADF complex.

Raman, XPS, WAXS and EXAFS characterizations

Since fullerene C_{60} is a powerful electron acceptor,[54] we investigated by Raman spectroscopy the possibility of electron transfer in the materials synthesized in toluene. Fig. 2 shows Raman spectra (532 nm) of T-Ru@C_{60} at different Ru/C_{60} ratio. The spectral range is mainly focus on the pentagonal pinch mode $A_g(2)$, because it have been proven that it is a reliable probe of metal fulleride polymer states. It is known that the energy of the $A_g(2)$ mode (1460 cm^{-1} for pure C_{60}) is sensitive to charge transfer in transition metal fullerides.[55]
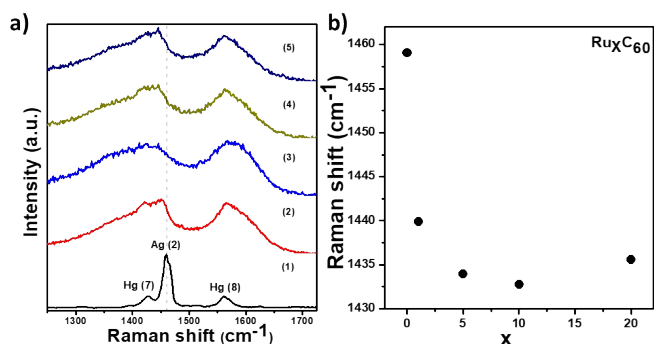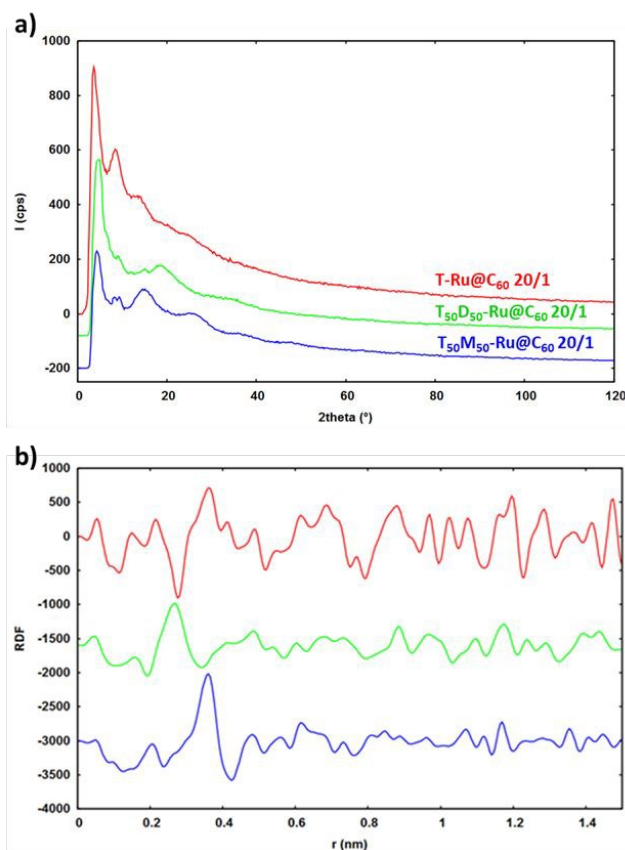
Fig. 2. a) Raman spectra of (1) C_{60}, (2) T-Ru@C_{60} 1/1, (3) T-Ru@C_{60} 5/1, (4) T-Ru@C_{60} 10/1 and (5) T-Ru@C_{60} 20/1; and b) Raman shift *vs.* Ru composition in C_{60} illustrates the broadening and down shift of $A_g(2)$ peak with respect to increase in Ru content.

We observe here a spectral shift as large as -16.2 cm^{-1} for the T-Ru@C_{60} 20/1 sample, and a significant broadening with increasing the amount of Ru, caused by strong electron-phonon interaction. Thus, a clear tendency can be observed where the displacement increases as the Ru content increases (Fig. 2b). It is commonly accepted that the $A_g(2)$ mode is downshifted by approximately 6 cm^{-1} transferred to C_{60} in alkali metal fulleride compounds.[56] The downshift of alkali metal fullerides depends of the number of metal atoms and each metal atom donates one electron to C_{60}, because there are only ionic bonds between C_{60} and alkali atoms. For transition metal fullerides, the relationship between shift and composition is more complex since these compounds exhibit a large proportion of covalent bonding between metal and C_{60}. However, a significant charge transfer is observed for our samples, suggesting the presence of electron deficient Ru species in the T-Ru@C_{60} series, as we had already shown for the D-Ru@C_{60} series.[27] The charge transfer from Ru to C_{60} was also evidenced by XPS (Fig. S9), by comparing the binding energy of $Ru_{3p3/2}$ (462.2 eV) with that of Ru^0 (461.2 eV). Raman[57] and XPS[58] signatures for charge transfer were already reported for Pd@C_{60} fullerides. DFT estimates of the charge transfer for various Ru_n@C_{60} models (n = 1, 2, 4, 13) confirm this general trend, with values from 0.1 (Ru_{13}@C_{60}) to 0.6 e$^-$ (Ru_1@C_{60}) per Ru center from Ru SA/clusters to neighboring C_{60} (Fig. S1). Further analyses were performed by WAXS in order to shed some light on the possible presence of metallic Ru clusters in the Ru@C_{60} hetero-structures. We first compared the $T_{50}D_{50}$-Ru@C_{60} and $T_{50}M_{50}$-Ru@C_{60} samples with the T-Ru@C_{60} sample at a similar Ru/C_{60} ratio of 20/1 (Fig. 3). For $T_{50}D_{50}$-Ru@C_{60}, a strong contribution can be observed at 0.267 nm in very good agreement with Ru-Ru metallic bond length (0.265 nm); confirming the presence of Ru clusters in this sample showing a core-shell structure (Fig. 1a). In the two other compounds, this distance could not be observed; however, they share a strong contribution close to 0.360 nm, likely also related to Ru-Ru distances but clearly non-bonding ones. A contribution in the 0.20-0.23 nm range is also observed for these two samples, which could be related to bonding of Ru with a light element (likely C, since Ru-C is close to 0.2 nm). We also analyzed the samples prepared in pure toluene at different Ru/C_{60} ratio (Fig. S10). As expected, for all

ratios, it was impossible to detect a metallic Ru_7Ru_A distance but a contribution in the 0.20-0.23 nm range could also systematically be observed. Finally, we compared the $T_{95}D_5$-Ru@C_{60} and $T_{95}M_5$-Ru@C_{60} samples with the T-Ru@C_{60} sample at a theoretical Ru/C_{60} ratio of 20/1 (Fig. S11). Differences could be observed between the different samples but poorly defined RDFs and extreme complexity make any analysis irrelevant beyond the observation of a similar distance in the 0.20-0.23 nm range strongly pointing to Ru-C bonding. Despite the difficulty to apply WAXS to these complex systems, in which both single atoms and few atom clusters may be present, it was possible from this technique to detect metallic Ru in $T_{50}D_{50}$-Ru@C_{60}. This complexity is confirmed by the simulated PDF profiles derived from the DFT models previously used to evaluate the charge transfer (Fig. S12), which are poorly comparable to the experimental profiles. It is however interesting to notice that no contribution at *ca.* 0.270 nm is observed for small clusters with a limited number of metallic Ru-Ru bonds on the simulated PDF profiles.

EXAFS analyses were also performed on the sample series prepared in pure toluene at different Ru/C_{60} ratio and on the $T_{95}M_5$-Ru@C_{60} sample. The $k^2\chi(k)$ and the corresponding Fourier Transforms (FTs) are reported in Fig. 4. A qualitative inspection of the FTs of the samples indicates that samples prepared in pure toluene show a single peak whose intensity increases with the Ru/C_{60} ratio.

Fig. 3. a) Diffractograms of $T_{50}D_{50}$-Ru@C_{60}, $T_{50}M_{50}$-Ru@C_{60} and T-Ru@C_{60} samples (Ru/C_{60} = 20/1); and b) related PDF.
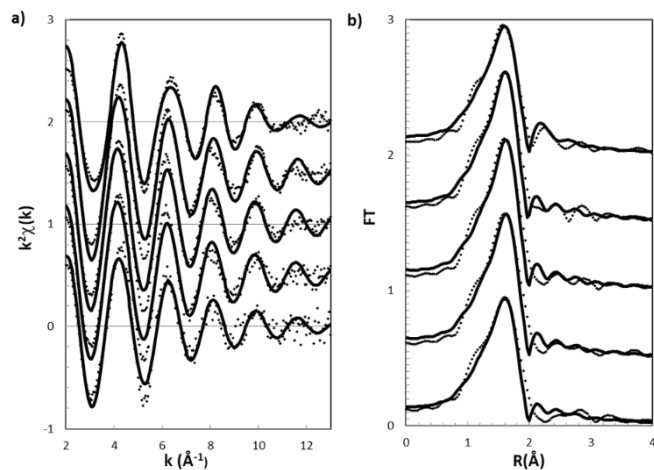

6 | *Catal. Sci. Technol.*, 2020, **00**, 1-3

This journal is © The Royal Society of Chemistry 20xx

Paper

Fig. 4. a) Fit of the EXAFS region; $k^2\chi(k)$; and b) corresponding FTs for T-Ru@C$_{60}$ 1/1, T-Ru@C$_{60}$ 5/1, T-Ru@C$_{60}$ 10/1, T-Ru@C$_{60}$ 20/1, and T$_{95}$M$_5$-Ru@C$_{60}$ 20/1 using toluene/methanol (from bottom to top). Dots: experiment; Fit: full line.

The sample prepared using toluene/methanol does show some differences, in that a hint of a second shell is detectable and the intensity of the peak is much lower than that of a sample produced using toluene with a comparable Ru/C$_{60}$ ratio. There is an additional difference in the position of the maximum that is slightly shifted to shorter distances, as also evidenced by the shift in the oscillations in the $k^2\chi(k)$. Data for all the samples were initially fitted with a single shell and a good fit was obtained with a Ru-C shell for all the samples. Ru-C coordination numbers are close to 8 for all samples (consistent with η^2-η^6 coordination), with the main difference for the sample made using toluene/methanol being a larger Debye-Waller factor. For this sample, the fit did improve by adding a second Ru-Ru shell. In Fig. 4 the fitting results are shown and the fitting parameters are reported in Table 2. It should be pointed out that, due to the small weight of the second Ru-Ru shell in the sample T$_{95}$M$_5$-Ru@C$_{60}$ and the strong correlation between coordination number and Debye-Waller factor, the values of the parameters reported in Table 2 can be

considered as purely indicative. Notwithstanding, the fit improvement provides a suggestion that Ru clusters could be incorporated in the T$_{95}$M$_5$-Ru@C$_{60}$ sample containing 34.7 % w/w of Ru. It is also worth mentioning that the EXAFS data reported for reduced Pt$_8$ clusters deposited on carbon black do have common features with our results.[59] For the sample prepared in pure toluene, the fact that only SA are produced with a well-defined environment (η^2-η^6 coordination) for Ru loading between 10 and 20% w/w is a remarkable result. Indeed, the challenges for SA catalysis for industrial applications are accurate control over the local structure of single sites and increasing the active-site density.[60] Currently the maximum loadings obtained for SA type catalysts are around 10% w/w.[61-63]

Catalytic activity of the Ru@C$_{60}$ nanostructures

Since STEM-HAADF observations and WAXS and EXAFS analyses were not decisive concerning the presence or not of Ru subnanometric particles in all the samples obtained with a mixture of solvents, we decide to use catalysis to probe their presence. Indeed, in hydrogenation reactions, the electron deficient Ru SA should be less efficient that Ru NP for hydrogen dissociative chemisorption, which is often rate limiting.[64] Thus, it was reported that among Pd$_n$C$_{60}$ fullerides, active hydrogenation compounds are those with n > 3,[65] that is the samples suspected to contain Pd NP.[30] We choose as first probe reaction the hydrogenation of nitrobenzene (Scheme 1) to aniline (AN), since Ru NP are known to be active for this reaction.[66-69] The reaction was studied at 30 bar H$_2$ and 80 °C in ethanol with a Ru concentration of 0.025 mmol. The specific activities are expressed as turnover frequency (h^{-1}). We independently checked that the C$_{60}$ fullerene has no activity for this reaction under these experimental conditions.

Table 3 shows the results obtained with the Ru@C$_{60}$ samples prepared in different solvents and at different Ru/C$_{60}$ ratio.

Table 2. Best fit parameters obtained by fitting the experimental EXAFS of samples. Coordination numbers (N), interatomic distances (R), Debye-Waller factors, ΔE_0 and R-factors are shown.

Sample		N	R(Å)	σ^2(Å^2)	ΔE_0	R-factor
T-Ru@C$_{60}$ 1/1	Ru-C	7.7±0.2	2.17 ± 0.02	0.006 ± 0.003	-3±2	0.037
T-Ru@C$_{60}$ 5/1	Ru-C	7.9±0.1	2.18 ± 0.01	0.005 ± 0.002	-4±1	0.040
T-Ru@C$_{60}$ 10/1	Ru-C	8.1±0.2	2.17 ± 0.02	0.005 ± 0.002	-4±2	0.039
T-Ru@C$_{60}$ 20/1	Ru-C	8.0±0.2	2.16 ± 0.02	0.005 ± 0.003	-4±2	0.039
T$_{95}$M$_5$-Ru@C$_{60}$ 20/1	Ru-C	8.0±0.2	2.16 ± 0.02	0.007 ± 0.002	-3±2	0.013
	Ru-Ru	2.7±0.2	2.67 ± 0.03	0.015 ± 0.004		

Paper
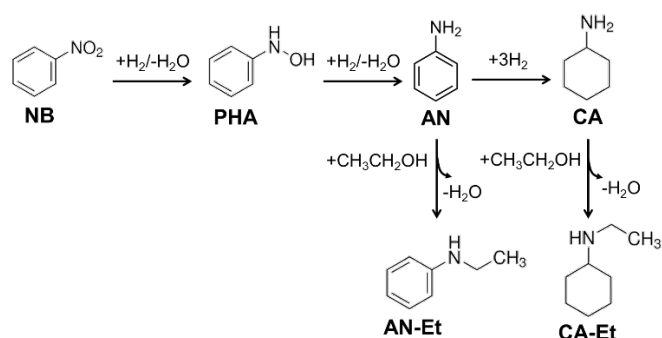
Scheme 1. Main products and byproducts formed during NB hydrogenation.

The main products of the reaction were AN and cyclohexylamine (CA). N-phenylhydroxylamine (PHA), and N-ethylaniline (AN-Et) and N-ethylcyclohexylamine (CA-Et) both formed by N-alkylation from ethanol, were the only detected by-products. All catalysts were found active for NB hydrogenation.

The evolution of the NB conversion over the time is shown in Fig. 5a for the Ru@C_{60} series prepared in toluene at different Ru/C_{60} ratio, and for the series prepared in toluene/methanol mixtures. For all the samples prepared in pure toluene (Ru/C_{60} ratio 1/1 to 20/1), for which only SA are present, the conversion of NB is low compared to the ones prepared in toluene/methanol mixtures. For these latter series, the activity increase is already observable for the $T_{95}M_5$-Ru@C_{60} sample, for which the presence of Ru clusters has been suggested from EXAFS analyses. The $T_{50}M_{50}$-Ru@C_{60} sample is by far the most active catalyst with a TOF of 135.5 h^{-1}. Comparison between samples prepared in pure toluene and in solvent mixtures are shown in Fig. 5b. The $T_{50}D_{50}$-Ru@C_{60} sample, for which metallic Ru has been evidenced by WAXS is much less efficient (TOF of 18.2 h^{-1}) than the $T_{50}M_{50}$-Ru@C_{60} sample (TOF of 135.5 h^{-1}). This result should be related to the core-shell structure of the $T_{50}D_{50}$-Ru@C_{60} catalyst, for which the active ruthenium is limited to the external surface of the spheres (Fig. 1a,b). In order to investigate the ability of various -(C_{60}-Ru$_n$-C_{60})$_n$-hetero-structures to chemisorb H$_2$ molecules, and thus get an idea on the activity of such metallic centers for further substrate hydrogenation, we have performed a series of calculations for naked Ru$_1$, and Ru$_2$, Ru$_4$ and Ru$_{13}$ clusters embedded in a 1D-C_{60} polymeric phase. Dissociative adsorption energy per H with respect to the H$_2$ molecule number in interaction with a Ru$_n$ cluster are shown in Fig. 6, as well as final geometry representations. Since for a Ru$_1$ SA, the 18 electron rule is satisfied upon the adsorption of 3 H$_2$ molecules, the adsorption energy drops and no further H$_2$ can be adsorbed.
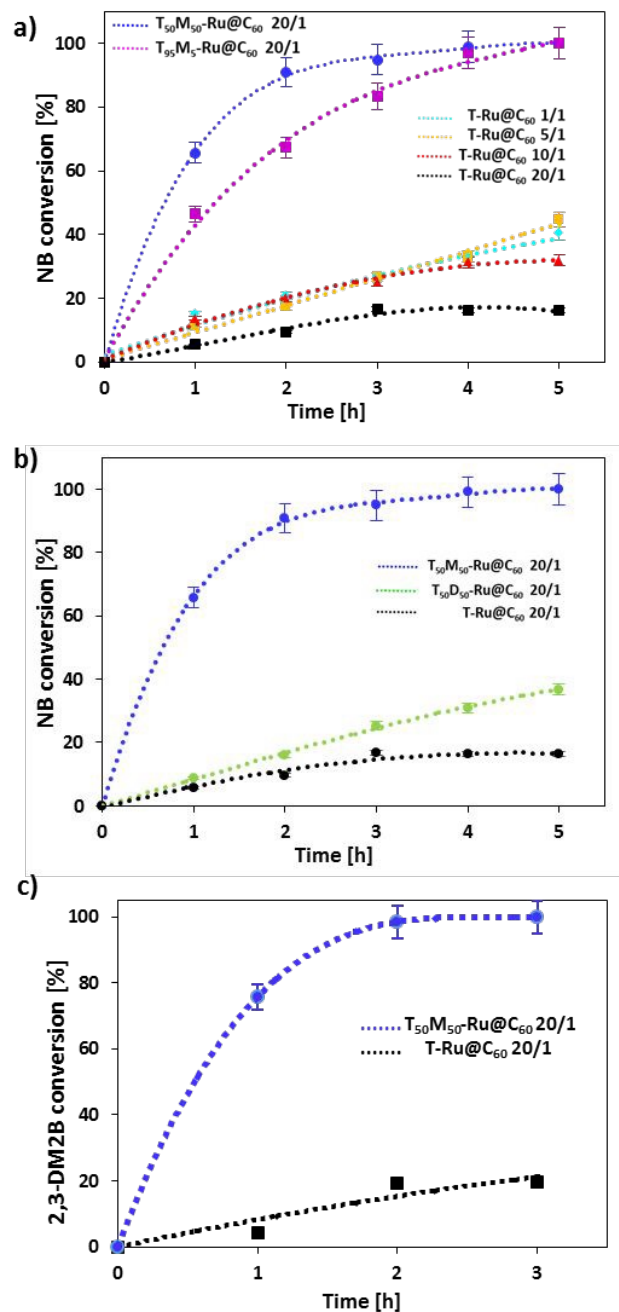
Fig. 5. Time-conversion curve for a) NB hydrogenation with T-Ru@C_{60} and TM-Ru@C_{60} materials; and b) T-Ru@C_{60} 20/1, $T_{50}M_{50}$-Ru@C_{60} and $T_{50}D_{50}$-Ru@C_{60}; and c) for 2,3-dimethyl-2-butene hydrogenation with T-Ru@C_{60} and $T_{50}M_{50}$-Ru@C_{60}.

Interestingly, the Ru center coordination mode, changes from η^2-η^6 to η^2-η^2 with 3 partially activated H$_2$ presenting elongated H-H bonds, around 0.9 Å (0.74 Å in H$_2$).

Paper

Table 3. Results of hydrogenation of nitrobenzene in ethanol with different Ru@C_{60} catalysts.

Ru/C_{60}	Nitro- group		Selectivity [%] [a]				
	TOF (h^{-1}) [b]	Time (h) [c]	AN	AN-Et	CA	CA-Et	PHA
T-Ru@C_{60} 1/1	14.5	2.3	82.4	8.5	7.1	2.0	-
T-Ru@C_{60} 5/1	15.0	2.2	85.3	4.6	-	-	10.1
T-Ru@C_{60} 10/1	13.4	2.5	78.4	6.4	5.5	3.6	2.9
T-Ru@C_{60} 20/1	12.5	3.0 [d]	86.7	5.4	3.1	-	4.9
$T_{95}M_5$-Ru@C_{60} 20/1	49.9	0.64	100.0	-	-	-	-
$T_{75}M_{25}$-Ru@C_{60} 20/1	107.36	0.34	83.5	-	-	2.9	13.6
$T_{50}M_{50}$-Ru@C_{60} 20/1	135.5	0.30	79.9	-	0.4	-	19.0
$T_{75}D_{25}$-Ru@C_{60} 20/1	12.6	2.5	75.9	14.3	-	-	8.8
$T_{50}D_{50}$-Ru@C_{60} 20/1	18.2	2.6	66.6	30.8	-	-	2.6

Reaction conditions: 0.025 mmol Ru, 500 mg (4.06 mmol) nitrobenzene, 200mg (1.1 mmol) dodecane (internal standard), 30 bar H_2, 80°C, 30 mL EtOH. [a] determined by GC-MS using internal standard technique at ≈ 20% of conversion. [b] TOF ($mol_{NBconverted}/mol_{Ru}.t$) calculated at ≈ 20% of conversion. [c] Time to reach 20% of conversion. [c] Time to reach 16% of conversion, which is de maximal obtained with this sample.

With larger clusters, more H_2 can be adsorbed and dissociated, but adsorption energy values always reach a plateau (around -5kcal/mol) for clusters smaller than Ru_{13}, experiencing a surface saturation effect. However, in the case of Ru_{13}, for a value of 1.5H/per surface Ru, a ratio usually reported experimentally,[70, 71] the energy per adsorbed H is still large and agrees well with previous reports.[72]

Fig. 6. Dissociative adsorption energy (in kcal/mol) per adsorbed H on various -(C_{60}-Ru_n-C_{60})$_n$- hetero-structures.
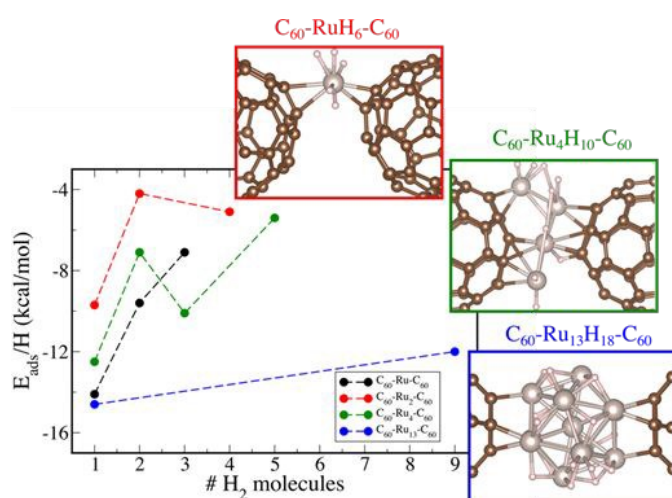
Those results strongly suggest that very electro-deficient Ru SA and few atom aggregates are not performing for H_2 activation compared to larger clusters. With larger clusters, more H_2 can be adsorbed and dissociated, but adsorption energy values always reach a plateau (around -5kcal/mol) for clusters smaller than Ru_{13}, experiencing a surface saturation effect. However, in the case of Ru_{13}, for a value of 1.5H/per surface Ru, a ratio usually reported experimentally,[70, 71] the energy per adsorbed H is still large and agrees well with previous reports.[72] Those results strongly suggest that very electro-deficient Ru SA and few atom aggregates are not performing for H_2 activation compared to larger clusters.

Finally, the high TOF obtained in NB hydrogenation compared to previous studies,[63, 66] incite us to evaluate the catalytic activity of the $T_{50}M_{50}$-Ru@C_{60} sample in the more difficult hydrogenation of the tetra-substituted olefin 2,3-dimethyl-2-butene. This reaction can be performed with cationic iridium complexes under mild conditions (room temperature, 1-5 bar, TOF = 4000 h^{-1}).[73-75] However, with some complexes irreversible deactivation process occurs, preventing reaction completion.[74] Colloidal metallic NP (Rh, Ru, Pt), although less active (TOF = 160-320 h^{-1}) are also efficient catalysts for this reaction under relatively mild conditions (room temperature to 75°C, 1-10 bar of H_2).[76, 77] As far as supported catalysts are concerned (Rh, Co), much lower activities were reported (TOF = 2-10 h^{-1}) under slightly harsher operating conditions (25 to 150°C, 5-40 bar).[78, 79] At 50°C and under 20 bar of H_2, the

Paper

reaction with the $T_{50}M_{50}$-Ru@C_{60} catalyst is completed within 2 h. The calculated TOF at 20% conversion 470 h^{-1} is to the best of our knowledge the higher ever reported for supported metallic NP. For this reaction also, the catalysts prepared in pure toluene containing only SA are much less active (Fig. 5c), pointing their low hydrogenation activity. Finally, we have performed a series of calculations to propose the mechanism of tetra-substituted olefin 2,3-dimethyl-2-butene hydrogenation. Interestingly due to the high steric hindrance induced by the small C_{60}-C_{60} distance, the hydrogenation is not possible on Ru SA. On $Ru_{13}H_{18}$, the hydrogenation reaction appears thermodynamically favorable, as it can be seen in Fig.7, with a negative balance of 26 kcal/mol with respect to the separated reactants. The regeneration of the catalyst leading to the release of the 2,3-dymethylbutane molecule and the coordination of a H_2 and 2,3-dimethyl-2-butene molecules is also favorable by -12 kcal/mol with respect to the final product (-38 kcal/mol with respect to the entrance channel). The first hydrogenation step leading to an alkyl intermediate is kinetically easily accessible with an activation barrier of 11 kcal/mol with respect to the π-coordinated adduct. On this intermediate it is interesting to note the presence of a β-agostic C-H interaction as evidenced by the H-Ru and H-C distances of 1.86 and 2.44 Å, respectively. The second step is a barrierless process with an energy barrier of less 2 kcal/mol leading to the formation of the 2,3-dimethylbutane product.

Conclusions

In conclusion, we have highlighted the crucial role of the solvent for the growth of subnanometric ruthenium nanoparticles in Ru@C_{60} hetero-structures. While Ru SA are selectively obtained in pure toluene (Ru@C_{60} hetero-structures with very high Ru loading = 9-20% w/w), the use of a toluene/methanol solvent mixture makes it possible to increase the metal loading up to 50% w/w and to obtain ruthenium clusters uniformly distributed in the materials. These novel catalysts are extremely active for the hydrogenation reactions of nitrobenzene and tetra-substituted 2,3-dimethyl-2-butene. For this latter reaction a TOF of 485 h^{-1} was calculated, which is the higher ever reported for supported metallic NP. This work provides a general strategy for producing high loading and ultra-dispersed supported catalyst for enhanced catalytic performance.

Fig. 7. A possible reaction path of 2,3-dimethyl-2-butene hydrogenation.
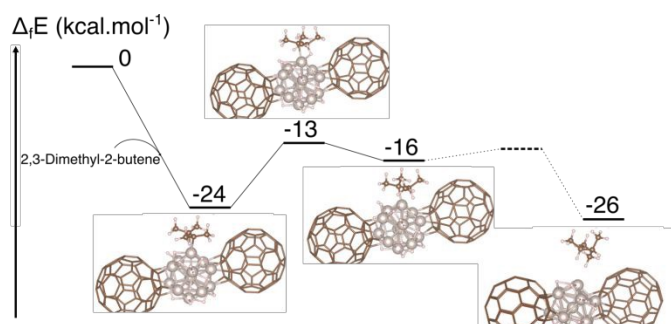
Conflicts of interest

There are no conflicts to declare.

Notes and references

1. J. Calvo Fuentes, J. Rivas and M. A. López-Quintela, in *Encyclopedia of Nanotechnology*, ed. B. Bhushan, Springer Netherlands, Dordrecht, 2012, pp. 2639-2648.
2. C. Rivera-Cárcamo and P. Serp, *ChemCatChem*, 2018, **10**, 5058-5091.
3. A. Wang, J. Li and T. Zhang, *Nature Reviews Chemistry*, 2018, **2**, 65-81.
4. J. Liu, *ACS Catalysis*, 2017, **7**, 34-59.
5. X.-F. Yang, A. Wang, B. Qiao, J. Li, J. Liu and T. Zhang, *Accounts of Chemical Research*, 2013, **46**, 1740-1748.
6. A. Mathew and T. Pradeep, *Particle & Particle Systems Characterization*, 2014, **31**, 1017-1053.
7. X. Yuan, X. Dou, K. Zheng and J. Xie, *Particle & Particle Systems Characterization*, 2015, **32**, 613-629.
8. J. M. Thomas, R. Raja and D. W. Lewis, *Angewandte Chemie International Edition*, 2005, **44**, 6456-6482.
9. H. Zhang, G. Liu, L. Shi and J. Ye, *Advanced Energy Materials*, 2018, **8**, 1701343.
10. Y.-B. Huang, J. Liang, X.-S. Wang and R. Cao, *Chemical Society Reviews*, 2017, **46**, 126-157.
11. H.-C. Zhou, J. R. Long and O. M. Yaghi, *Chemical Reviews*, 2012, **112**, 673-674.
12. L. Jiao and H.-L. Jiang, *Chem*, 2019, **5**, 786-804.
13. G. Li and R. Jin, *Accounts of Chemical Research*, 2013, **46**, 1749-1758.
14. K. S. Krishna, J. Liu, P. Tarakeshwar, V. Mujica, J. J. Spivey and C. S. S. R. Kumar, in *Atomically-Precise Methods for Synthesis of Solid Catalysts*, The Royal Society of Chemistry, 2015, pp. 87-122.
15. A. Ghosh and T. Pradeep, *European Journal of Inorganic Chemistry*, 2014, 5271-5275.
16. Z. Wu, M. A. MacDonald, J. Chen, P. Zhang and R. Jin, *Journal of the American Chemical Society*, 2011, **133**, 9670-9673.
17. Y. Zhu, H. Qian and R. Jin, *Journal of Materials Chemistry*, 2011, **21**, 6793-6799.
18. I. Chakraborty and T. Pradeep, *Chemical Reviews*, 2017, **117**, 8208-8271.
19. R. Jin, *Nanoscale*, 2015, **7**, 1549-1565.
20. K. Okamoto, R. Akiyama, H. Yoshida, T. Yoshida and S. Kobayashi, *Journal of the American Chemical Society*, 2005, **127**, 2125-2135.

10 | *Catal. Sci. Technol.*, 2020, **00**, 1-3

This journal is © The Royal Society of Chemistry 20xx

Nanoscale

Paper

21. E.-Y. Zhang and C.-R. Wang, *Current Opinion in Colloid & Interface Science*, 2009, **14**, 148-156.

22. J. Goclon, K. Winkler and J. T. Margraf, *RSC Advances*, 2017, **7**, 2202-2210.

23. A. L. Balch, K. Winkler, *Chemical Reviews*, 2016, **116**, 3812–3882.

24. H. Nagashima, A. Nakaoka, Y. Saito, M. Kato, T. Kawanishi and K. Itoh, *Journal of the Chemical Society, Chemical Communications*, 1992, 377-379.

25. A. V. Talyzin, A. Dzwilewski and M. Pudelko, *Carbon*, 2007, **45**, 2564-2569.

26. J. M. Cowley, M. Q. Liu, B. L. Ramakrishna, T. S. Peace, A. K. Wertsching and M. R. Pena, *Carbon*, 1994, **32**, 746-748.

27. F. Leng, I. C. Gerber, P. Lecante, W. Bacsa, J. Miller, J. R. Gallagher, S. Moldovan, M. Girleanu, M. R. Axet and P. Serp, *RSC Advances*, 2016, **6**, 69135-69148.

28. A. S. Lobach, B. P. Tarasov, Y. M. Shul'ga, A. A. Perov and A. N. Stepanov, *Russian Chemical Bulletin*, 1996, **45**, 464-465.

29. E. Brancewicz, E. Grądzka, A. Basa and K. Winkler, *Electrochimica Acta*, 2014, **128**, 91-101.

30. O. Loboda, V. R. Jensen and K. J. B⌀rve, *Fullerenes, Nanotubes and Carbon Nanostructures*, 2006, **14**, 365-371.

31 V. A. Chernov, V. N. Ivanova, A. N. Kozhevnikova, G. A. Mardezhova, S. G. Nikitenko and A. A. Nikiforov, *Nuclear Instruments and Methods in Physics Research Section A: Accelerators, Spectrometers, Detectors and Associated Equipment*, 1995, **359**, 250-253.

32. K. Lee, H. Song and J. T. Park, Accounts of Chemical Research, 2003, **36**, 78-86.

33. N. Goldberg and R. Hoffmann, *Inorganic Chemistry*, 1996, **35**, 4369-4377.

34. B. Ravel and M. Newville, *Journal of Synchrotron Radiation*, 2005, **12**, 537-541.

35. G. Kresse and J. Hafner, *Physical Review B*, 1993, **47**, 558-561.

36. G. Kresse and J. Furthmüller, *Physical Review B*, 1996, **54**, 11169-11186.

37. G. Kresse and J. Furthmüller, *Computational Materials Science*, 1996, **6**, 15-50.

38. G. Kresse and J. Hafner, *Physical Review B*, 1994, **49**, 14251-14269.

39. P. E. Blöchl, *Physical Review B*, 1994, **50**, 17953-17979.

40. G. Kresse and D. Joubert, *Physical Review B*, 1999, **59**, 1758-1775.

41. J. P. Perdew, K. Burke and M. Ernzerhof, *Physical Review Letters*, 1996, **77**, 3865-3868.

42. G. Henkelman, A. Arnaldsson and H. Jónsson, *Computational Materials Science*, 2006, **36**, 354-360.

43. W. Tang, E. Sanville and G. Henkelman, *Journal of Physics: Condensed Matter*, 2009, **21**, 084204.

44. G. Henkelman, *Journal of Chemical Physics*, 2000, **113**, 9901-9904.

45. G. Henkelman, H. Jónsson, *Journal of Chemical Physics*, 2000, **113**, 9978-9985.

46. M. Sathish, K. i. Miyazawa, J. P. Hill and K. Ariga, *Journal of the American Chemical Society*, 2009, **131**, 6372-6373.

47. X. Zhang, X. Gong, Y. Sun, M. Xu, B. Xi, X. Zhao, X. Ye, X. Yao, M. He, L. Liu, Y. Liu, *Journal of Physical Chemistry C* 2019, **123**, 30571–30577.

48. M. Zhu and D. Vesely, *European Polymer Journal*, 2007, **43**, 4503-4515.

49. A. Hayashi, S. Yamamoto, K. Suzuki, T. Matsuoka, *Journal of Materials Chemistry*, 2004, **14**, 2633–2637.

50. P. Pertici, G. Vitulli, R. Lazzaroni, P. Salvadori and P. L. Barili, *Journal of the Chemical Society, Dalton Transactions*, 1982, 1019-1022.

51. M. Bown and J. M. Waters, *Journal of the American Chemical Society*, 1990, **112**, 2442-2443.

52. M. Kawai, H. Yuge and T. K. Miyamoto, *Acta Crystallographica Section C*, 2002, **58**, m581-m582.

53. S. Mane, *Canadian Chemical Transactions*, 2016, **4**, 210-225.

54. R. C. Haddon, R. E. Palmer, H. W. Kroto and P. A. Sermon, *Philosophical Transactions: Physical Sciences and Engineering*, 1993, **343**, 53-62.

55. S. J. Chase, W. S. Bacsa, M. G. Mitch, L. J. Pilione and J. S. Lannin, *Physical Review B*, 1992, **46**, 7873-7877.

56. K.-A. Wang, Y. Wang, P. Zhou, J. M. Holden, S.-l. Ren, G. T. Hager, H. F. Ni, P. C. Eklund, G. Dresselhaus and M. S. Dresselhaus, *Physical Review B*, 1992, **45**, 1955-1958.

57. A. V. Talyzin and U. Jansson, *Thin Solid Films*, 2003, **429**, 96-101.

58. K. Winkler, K. Noworyta, A. de Bettencourt-Dias, J. W. Sobczak, C.-T. Wu, L.-C. Chen, W. Kutner and A. L. Balch, *Journal of Materials Chemistry*, 2003, **13**, 518-525.

59. T. Imaoka, Y. Akanuma, N. Haruta, S. Tsuchiya, K. Ishihara, T. Okayasu, W.-J. Chun, M. Takahashi, K. Yamamoto, *Nature Communications*, 2017, **8**, 688.

60. J. Wang, Z. Li, Y. Wu and Y. Li, *Advanced Materials*, 2018, **30**, 1801649.

61. L. Zhao, Y. Zhang, L.-B. Huang, X.-Z. Liu, Q.-H. Zhang, C. He, Z.-Y. Wu, L.-J. Zhang, J. Wu, W. Yang, L. Gu, J.-S. Hu and L.-J. Wan, *Nature Communications*, 2019, **10**, 1278.

62. J. Li, S. Chen, N. Yang, M. Deng, S. Ibraheem, J. Deng, J. Li, L. Li and Z. Wei, *Angewandte Chemie International Edition*, 2019, **58**, 7035-7039.

63. J. Wu, L. Xiong, B. Zhao, M. Liu and L. Huang, *Small Methods*, 2020, **4**, 1900540.

64. M. D. Rossell, F. J. Caparrós, I. Angurell, G. Muller, J. Llorca, M. Seco and O. Rossell, *Catalysis Science & Technology*, 2016, **6**, 4081-4085.

65. N. F. Goldshleger, *Fullerene Science and Technology*, 2001, **9**, 255-280.

66. F. Leng, I. C. Gerber, P. Lecante, S. Moldovan, M. Girleanu, M. R. Axet and P. Serp, *ACS Catalysis*, 2016, **6**, 6018-6024.

67. M. R. Axet, S. Conejero and I. C. Gerber, *ACS Applied Nano Materials*, 2018, **1**, 5885-5894.

68. F. Leng, I. C. Gerber, P. Lecante, A. Bentaleb, A. Muñoz, B. M. Illescas, N. Martín, G. Melinte, O. Ersen, H. Martinez, M. R. Axet and P. Serp, *Chemistry – A European Journal*, 2017, **23**, 13379-13386.

69. C. S. Srikanth, V. P. Kumar, B. Viswanadham, A. Srikanth and K. V. R. Chary, *Journal of Nanoscience and Nanotechnology*, 2015, **15**, 5403-5409.

70. J. García-Antón, M. R. Axet, S. Jansat, K. Philippot, B. Chaudret, T. Pery, G. Buntkowsky and H.-H. Limbach, *Angewandte Chemie International Edition*, 2008, **47**, 2074-2078.

71. R. Berthoud, P. Délichère, D. Gajan, W. Lukens, K. Pelzer, J.-M. Basset, J.-P. Candy and C. Copéret, *Journal of Catalysis*, 2008, **260**, 387-391.

This journal is © The Royal Society of Chemistry 20xx

Catal. Sci. Technol., 2020, **00**, 1-3 | **11**

72. L. Cusinato, L. M. Martínez-Prieto, B. Chaudret, I. del Rosal and R. Poteau, *Nanoscale*, 2016, **8**, 10974-10992.
73. R. H. Crabtree, H. Felkin and G. E. Morris, *Journal of Organometallic Chemistry*, 1977, **141**, 205-215.
74. R. Crabtree, *Accounts of Chemical Research*, 1979, **12**, 331-337.
75. L. D. Vázquez-Serrano, B. T. Owens and J. M. Buriak, *Chemical Communications*, 2002, 2518-2519.
76. L. Gao, K. Kojima and H. Nagashima, *Tetrahedron*, 2015, **71**, 6414-6423.
77. E. T. Silveira, A. P. Umpierre, L. M. Rossi, G. Machado, J. Morais, G. V. Soares, I. J. R. Baumvol, S. R. Teixeira, P. F. P. Fichtner and J. Dupont, *Chemistry – A European Journal*, 2004, **10**, 3734-3740.
78. F. K. Scharnagl, M. F. Hertrich, F. Ferretti, C. Kreyenschulte, H. Lund, R. Jackstell and M. Beller, *Science Advances*, 2018, **4**, eaau1248.
79. A. Sánchez, M. Fang, A. Ahmed and R. A. Sánchez-Delgado, *Applied Catalysis A: General*, 2014, **477**, 117-124.

12 | *Catal. Sci. Technol.*, 2020, **00**, 1-3

This journal is © The Royal Society of Chemistry 20xx

Paper